RELATION BETWEEN CHEMISTRY, SOLIDIFICATION BEHAVIOUR, MICROSTRUCTURE AND MICROPOROSITY IN NICKEL-BASE SUPERALLOYS

J. Lecomte-Beckers

Department of Metallurgy and Materials Science
Faculty of Applied Science, University of Liège
Hall de Métallurgie, Sart Tilman, B17
Liège, Belgium

Abstract

Microporosity formation in nickel-base superalloys is studied experimentally and theoretically. A microporosity index, ΔP^*, which depends on solidification parameters and alloy properties has been deduced. This index can be determined from parameters obtained by quantitative differential thermal analysis. The effect of mean alloying elements on the formation of microporosity is evaluated. Thus, aluminum, titanium and cobalt are found to increase and chromium to decrease microporosity. The effect of carbon depends on aluminum content and can be beneficial or detrimental.

Superalloys 1988
Edited by S. Reichman, D.N. Duhl,
G. Maurer, S. Antolovich and C. Lund
The Metallurgical Society, 1988

Introduction

Gas turbine components of complex geometry such as blades are currently produced by the technique of investment casting. Thus the microstructure and associated mechanical properties depend on solidification sequence although modifications can be introduced by the subsequent heat treatments. One of the solidification variables influencing mechanical properties is microporosity. This microporosity may result from shinkage, dissolved gases or a combination of both. However it must be noted that the gas content of modern superalloys is generally kept low and that most of it is either chemically bounded or kept into solution (1).

Microporosity is mostly caused by solidification shrinkage. It is well known that microporosity formation in nickel-base superalloys can be greatly affected by the casting conditions and by the chemical compositions of the melt. These parameters are not independent and influence deeply the solidification sequence which is the determinent factor in microporosity formation.

The aim of this work was to study superalloy proneness to microporosity in relation with solidification behavior and to point out the influence of the six major alloying elements : carbon, chromium, cobalt, molybdenum, titanium and aluminum.

Basic considerations on the mechanism of microporosity formation have led to a theoretical model. This one is based on pressure drop evaluation in the interdendritic liquid and introduce the so called ΔP^* coefficient which makes use of several solidification features (2)(3). Some parameters contained in this model are related to solidification sequence and have been extensively studied (4). This ΔP^* coefficient can only be computed if the evolution of the liquid fraction with time or with temperature is accurately known. Therefore we have developed a quantitative analysis of DTA based on the fact that peak intensity is proportional to transformation rate (2) (3). It is then possible to derive formulas giving solid and liquid fractions and solidification enthalpy (3).

Basic considerations on the mechanisms of microporosity formation have been summarized in the next section to introduce our experimental analysis of solidification behaviour which is presented in the following sections along with our main results and conclusions.

Basic considerations on microporosity formation

Nickel-base superalloys contract on solidifying. Most of this contraction takes place when efficient feeding mechanisms are still operative : liquid and mass feeding (6). However mass feeding lose efficacity when about 70% of the alloy is solidified ; capillarity (interdendritic or intergranular) feeding then becomes the only operative feeding mode. Microporosity formation occurs during the last stages of solidification when capillarity feeding becomes insufficient. Micropores form mainly because of the pressure drop resulting from flow of fluid through the liquid-solid mushy zone, which counterbalances the atmospheric pressure acting on the dendrite top (7). Microporosity occurs when the local pressure $p(x)$ drops below some critical value which may be predicted from nucleation theory (8).

The local pressure in the mushy zone during dendritic solidification have been calculated using the fluid flow calculations available for porous media, i.e. the interdendritic flow velocity obeys Darcy law and is

linearly related to gravity and pressure variation (7)(8)(9).

Using the Darcy law :

$$\underline{V}_L = - \frac{K}{\mu f_L} (- \underline{\nabla} p + \rho_L \underline{g})$$

where : $\underline{V}_L$ is the interdendritic liquid velocity
K is the permeability of the porous material
μ is the viscosity of the liquid moving through it
ρ_L is the interdendritic liquid viscosity
$\underline{g}$ is the gravity acceleration
f_L is the liquid fraction.

the law of continuity and the generally accepted relation

$$K(x) = \gamma f^2_L(x)$$

where γ is a constant depending on dendrite structure

$$\gamma = \frac{1}{24} \pi n \tau^3$$

where n is the dendrite number density, and
τ the tortuosity of the interdendritic channels (9),

lead to an analytic expression of the local pressure in interdendritic channels (2)(3).

This local pressure results from atmospheric effect and pressure drop in interdendritic channels. The pressure drop is related to the evolution of the liquid fraction along the interdendritic channels of the mushy zone. Experimental data obtained using quantitative analysis of DTA charts show that liquid fraction can be fairly approximated by a linear law over a substantial portion of the mushy zone (2)(3). This analysis leads to the definition of the microporosity index ΔP^*(2)(3). A high ΔP^* value correspond to an important tendency for defects formation while a low ΔP^* is related to less defects formation. This microporosity index ΔP^* may be expressed by :

$$\Delta P^* = \frac{24 \mu \beta' n \tau^3}{\rho_L g} \left(\frac{\Delta T}{G^2} \right) \left(\frac{df_S}{dt} \right)$$

The typical meaning of this parameter is straightforward. It suggests that internal soundness is favoured by a short solidification range ΔT, low dendrite number density n and "tortuosity" τ^3, high interdendritic liquid density ρ_L and fluidity, high thermal gradient G, low solidification rate df_S/dt and small contraction β' ($\beta' = \rho_S - \rho_L / \rho_L$).

Experimental procedure

Choice and Preparation of the Alloys.

Eight experimental alloy compositions were chosen following factorial design of 2^3 experiments to study the influence of the six major elements, each used at only two nominal contents (table I). The elements carbon, chromium and cobalt have been chosen as main factors, and the elements molybdenum, titanium and aluminum have been identified with the two-factor interactions.

The three-factor interaction was used to estimate σ, the experimental error. Statistical significance of the element effects was tested by an F-test (analysis of variance) and the level of significance of the effects was fixed at 10%. The significant effects are framed in the table presented.

The experimental alloys were elaborated under vacuum in an induction furnace. After homogenization, the liquid alloys were cast into preheated cylindrical sillimanite molds. These cylindrical rods were used for microstructural characterizations and DTA measurements. They were also subsequently turned to adequate specimen dimensions for QDS experiments.

Directionaly Solidified and Quenched Samples

The major part of this investigation was conducted on directionally solidified and quenched samples (Q.D.S.). This technique of unidirectional growth interrupted by quenching of the remaining liquid at a given moment offers a convenient way of studying the microstructure of the solid during solidification, as well as after its completion. It allows a fairly easy control of the two important parameters : thermal gradient and solidification rate.

The turned sample was contained in an alumina crucible (0.006m diam x 0.015m long) which is placed on a bottom water-cooled chill. This assembly was withdrawn at a constant rate R (0.060 mh^{-1}) from an induction furnace equiped with a graphite suceptor. The temperature of the sample was recorded by a second thermocouple placed at the central axis of the sample, in the solidified part which will be melted and unirectionally solidified.

The sample was melted under vacuum and superheated by 120°C above the equilibrium temperature, which was determined by DTA (4). After the temperature equilibrium was attained the crucible was withdrawn.

When steady state was established the width of the mushy zone as well as the temperature profile in the sample was stationnary with respect to the furnace and the grow rate of the solid in the heat flow was equal to the rate at which the crucible was withdrawn. The average thermal gradient in the solid-liquid region was determined from the temperature-distance charts and was $1 \times 10^{4} °Km^{-1}$. Under these steady-state growth conditions, solidification was dendritic. Growth of the dendritic specimen was interrupted at a given moment by quenching the remaining liquid achieved by pneumatically pulling the crucible from the furnace at very high speed (1m/s) and simultaneously cooling it with the helium jet.

Table I - Factorial design

EXPERIMENTS	A % C	B % Cr	C % Co	C(=AB) % Mo	E(=AC) % Ti	F(=BC) % Al	ALLOY NUMBER	ELEMENT TESTED
1 (def)	0.06	7.9	0	4	4.6	5.4	I	-
a (f)	0.14	7.5	0	0.5	1	5.5	II	carbon
b (e)	0.05	12	0	0.5	4.7	2.2	III	chromium
ab (d)	0.14	11.7	0	4	1	2.2	IV	molybdenum
c (d)	0.05	7.7	11.7	4	1	2.0	V	cobalt
ac (e)	0.15	8	10.2	0.5	4.6	2	VI	titanium
bc (f)	0.04	11.7	10.3	0.6	1.1	4.8	VII	aluminum
abc (def)	0.16	12	10.7	3.9	4.6	5.1	VIII	-

Metallographic Preparation

Each directionally solidified sample was sectioned longitudinally, polished and etched to study morphological features of the mushy zone. Transverse sections taken within the mushy zone, in the zone which was completely solidified at the moment of quench, were used to measure microporosity.

Morphological analyses were performed on transverse sections after appropriate etching on a (Quantimet 720) computerized image analyser. Forty-nine fields were analyzed on each sections. At each field (7 x 5 mm^2) corresponded 500.000 pixels.

Differential Thermal Analysis

Small cubic samples, approximately 0.3g in weight, were taken from each master rods and subjected to Differential Thermal Analysis (DTA) against a Pt reference. The tests were carried out under the protection of a constant argon flow (300ml/min) at a constant heating and cooling rate λ (600°C/h, peak temperature of 1450°C), corresponding to QDS experiments cooling rate, to observe the solidification sequence.

Results

Microporosity

Microporosity was measured in sectioned QDS samples. Quantitative measurements have been performed in the zone which was completely solidified at the moment of quench and the surface fraction was measured (total micropore area divided by total area examined). This parameter was choosen because it combines number and size of micropores present.

Comparison with the model

The predictions suggested by ΔP^* have been compared to the experimental results. This ΔP^* calculated is in good correlation with the measured surface fraction of micropores (fig.1) : for most of the alloys the level of the ΔP^* corresponds well to the surface fraction of the micropores.

Discussion on the effects of the alloying elements on the microporosity index parameters

This microporosity index depends on several parameters :

1) μ : viscosity of interdendritic liquid.
This viscosity is strongly influenced by the effect of segregation and precipitation during solidification. It is difficult to calculate accurately the value of this term but it can be evaluated in relation with the total enthalpy which is determined by quantitative DTA. It can be assumed that for an identical solid fraction, the liquid temperature is higher in the alloy with the highest enthalpy and its liquid viscosity is less.

2) β' : solidification shrinkage $\beta' = \dfrac{\rho_S - \rho_L}{\rho_L}$

ρ_S and ρ_L are the densities of the solid and liquid, respectively.

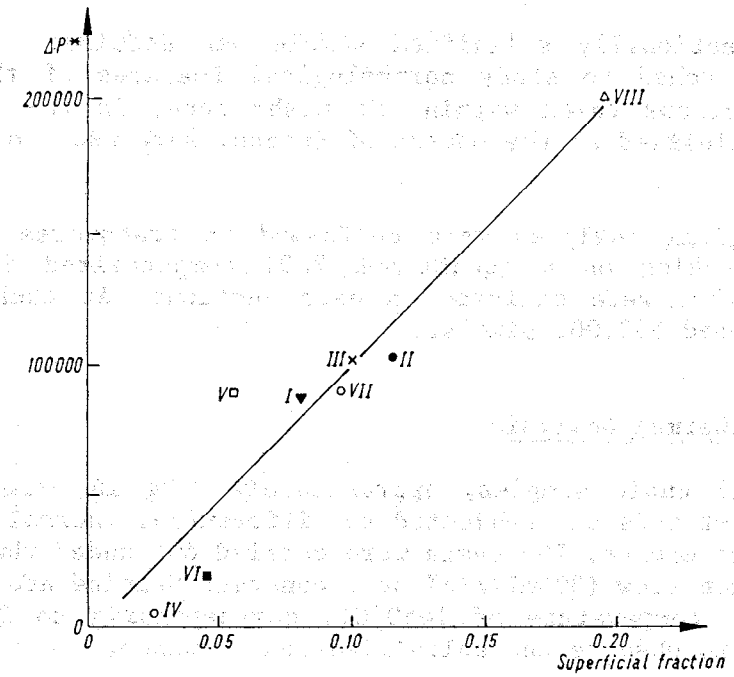

Figure 1 - Correlation between ΔP* and micropore surface fraction (to appear in Met. Trans.)

In the interdendritic channels the remaining liquid near the end of the solidification is always enriched in titanium and molybdenum (important for alloys containing cobalt), chromium and aluminum (for alloys rich in aluminum) and impoverished in cobalt when compared with the dendritic solid (4).

It is assume that the shrinkage coefficient obeys linear law of mixtures and is the combination of the shrinkage of each element remaining in the liquid. Moreover β' depends on the coefficient of linear thermal expansion.

Knowing the linear thermal expansion coefficient it is assumed that a nickel solid solution exhibits a high β' when poor in titanium, chromium and molybdenum and mostly rich in aluminum.

3) n : number of interdendritic channels per unit area.
In first approximation this can be assimilated to the number of dendrites per unit area which can be measured metallographically on QDS transverse sections.

4) τ : "tortuosity" of the dendrites.

It is an estimation of the importance of secondary dendrite arms of the dendrites. This factor can be evaluated metallographically on transverse sections. It can also be determined by quantitative DTA tests which gives the solidification curve (i.e. the fraction of solid in relation with time or temperature). The approach used has been described in details elsewhere (2)(3).

It has been shown that the shape and tortuosity of the dendrite structure obtained on QDS samples were strongly depending on the evolution of the parameter $1/\lambda \ df_s/dt$ (λ is the DTA cooling rate) during solidification. The initial increase of this parameter relates to dendrite growth and its subsequent shape after the maximum, to dendrite coarsening. More precisely, a high peak value at a high solid fraction corresponds to

smooth dendrites, whereas a low peak values at a lower solid fraction favours growh rathes than coarsening and is indicative of a more tortuous dendrite structure (2) (3).

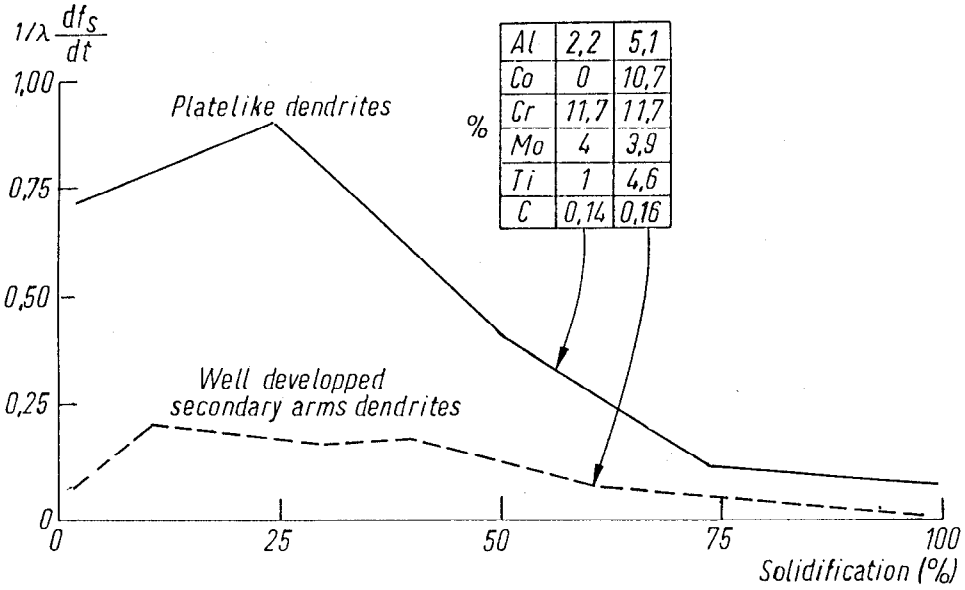

Figure 2 - Evaluation of normalised solidification rate

5) g : gravity acceleration considered as a constant.

6) ΔT : solidification range, determined by DTA.

7) G : thermal gradient in the mushy zone, constant in QDS experiments.

8) $(\frac{dfs}{dt})$: average solidification rate at the end of solidification calculated by quantitative DTA.

Table II shows the results of the factorial analysis of the various parameters n, τ^3, df_S/dt ΔT, ΔH. It must be kept in mind that the influence of ΔT and τ^3 (which have a high value) is more important than that of n, and df_S/dt ones.

Table II - Effects of alloying elements on the parameters used in ΔP^*

	n	τ	$(\frac{df_S}{dt})_{end}$	ΔT	ΔH	β'
Carbon	↓	⇓	↓	⇑	↑	–
Chromium	↓	↓	↑	↑	↑	⇓
Molybdenum	↑	↓	⇑	↓	↓	⇓
Cobalt	↑	⇑	↓	↑	↑	–
Titanium	⇓	⇑	⇓	⇑	↓	⇓
Aluminum	↓	⇑	↓	⇑	⇓	⇑

It can be seen that :

1) Aluminum is detrimental because it widens the equilibrium solidification range ΔT, raises the contraction β' and decreases the viscosity

μ of the liquid metal by decreasing ΔH, the total enthalpy.

2) Chromium possesses some beneficial effect by decreasing β'.

3) Cobalt is detrimental because it increases the tortuosity.

4) Titanium is detrimental because it widens the solidification range and increases the tortuosity but it is favorable by decreasing the number density of dendrites, the shrinkage coefficient β' and the parameter (df_S/dt) end.

5) Molybdenum is detrimental because it increases the parameters (df_S/dt) end but possesses a beneficial effect by decreasing β'.

6) Carbon is detrimental because it widens the equilibrium solidification range ΔT but it seems to be favorable in decreasing the tortuosity. An interaction between aluminum and carbon may lead to a favourable effect if aluminum is low and vice versa (table III).

Table III - Combined influence of carbone and aluminum on micropore surface fraction

Alloy	Aluminum	Carbon	Micropore surface fraction
I	5.5	0.05	0.081
II	5.5	0.15	0.131
III	2	0.05	0.101
IV	2	0.15	0.025
V	2	0.05	0.055
VI	2	0.15	0.046
VII	5.5	0.05	0.095
VIII	5.5	0.15	0.188

Acknowledgements

The author expresses her deep gratitude to CRM (Centre de Recherches Métallurgiques - Belgique) and IRSIA (Institut pour la Recherche Scientifique dans l'Industrie et l'Agriculture - Belgique) for support of this work. A sincere appreciation is extended to Mr. D. Coutsouradis and particularly to Dr. M. Lamberigts of CRM for providing support and evaluable comments.

Thanks are also due to Professor T.Z. Kattamis, University of Connecticut for helpful discussions.

References

1. S. Rupp, Y. Bienvenu, J. Massol. Rapport final-actions concertées Cost-50/III, Novembre 84, Ecole des Mines de Paris, France.

2. J. Lecomte-Beckers, M. Lamberigts. Proceedings of "High temperature alloys for gas turbine and other applications 1986", vol.I, pp.745-757. Ed. D. Reidel Publishing Co, Dordrecht, The Netherlands, 1986.

3. J. Lecomte-Beckers. "Study of microporosity formation in nickel-base superalloys". Metall. Trans. (to be published).

4. J. Lecomte-Beckers. "Study of solidification features of nickel-base superalloys in relation with composition". Metall. Trans. (to be published).

5. H. Fredriksson, G. Rogberg. Metal Science, December 1979, 685-690.

6. J. Campbell. The British Foundryman, April 1969, p.147.

7. R. Mehrabian, M. Keane, M.C. Flemings. Metall.Trans., 1970, vol.1, 1209.

8. D. Apelian, M.C. Flemings, R. Mehrabian. Metall.Trans., 1974, vol.5, 2533.

9. M.C. Flemings. Solidification processing, Materials Science and Engineering Series. Mc Graw Hill, USA, 1974.